CHAPTER-4
Investigating Optical, Structural and Morphological Properties of Polycrystalline CdTe Thin-film Deposited by RF Magnetron Sputtering

Chapter 4

4.1 Introduction

Cadmium Telluride (CdTe) shows excellent applicability for optoelectronic and photonic devices due to its crucial properties such as long term performance stability [252], direct bandgap (1.44eV) that is close to the optimum value for solar energy conversion [253], and high absorption coefficient (>10^5 cm^{-1}) in the visible region [254, 255] and In particular, II–VI semiconductor-multilayer structures have recently attracted enormous interest as being suitable for various photovoltaic devices [110]. Up to now a survey of literature shows that various deposition techniques have been developed to obtain the optimizing the physical properties of CdTe thin films, among which pulsed laser deposition (PLD) [256, 257], closed vapor transport [53, 258], molecular beam epitaxy (MBE) [259], electrodeposition [260], metalorganic chemical vapor deposition (MOCVD) [261], successive ionic layer adsorption and reaction method (SILAR) [262], screen printing [263], spray pyrolysis [53], and vacuum evaporation [264, 265] are worth mentioning. RF magnetron sputtering permits deposition at low temperatures and gives better adhesion, larger coverage, and higher film density than other methods. In this chapter, Radiofrequency (RF) magnetron sputtering method is used to form CdTe thin films by varying two parameters such as RF power and N_2 concentrations for optimizing the structural and optical properties to use as a suitable candidate for solar cell applications.

We demonstrated the synthesis and characterization of CdTe films using the RF magnetron sputtering method. Structural, electrical, and optical properties of CdTe films deposited by RF magnetron sputtering method were obtained via computational calculations. Calculations were illustrated, in terms of the variation in grain size, roughness, and optical characteristics of CdTe. Moreover, the influences of changing RF power and post-

annealing treatment on the physical properties of the films are studied and the theoretical result found to agree with the experimental results. In the comparative study of CdTe thin film of varying two parameters we investigate that at 100W and 2% N_2 has an optimum bandgap i.e. 1.58 eV because of the optical and structural properties, it can be used as an absorber material for solar cell applications.

4.2 Experimental details

4.2.1 Film Preparation

Here, we have synthesized a series of CdTe thin films via RF magnetron sputtering (Kurt J. Lesker Co) under controlled growth conditions of various thickness by varying two parameters like RF power and nitrogen concentration. A CdTe target (99.999% purity) was used as a sputtering source. The glass substrates were prepared with a standard cleaning procedure using organic solvents before being etched in HCl for 30 s. Finally they were rinsed for 15 min in de-ionized water, and dried with nitrogen fuel to cast off surface contamination. The CdTe films were deposited on substrates using an indigenously designed locally fabricated RF magnetron sputtering system. Figure 4.1 shows the schematic diagram of the RF magnetron sputtering system.

Figure 4.1. Schematic diagram of indigenously designed locally fabricated RF magnetron sputtering system

It includes a cylindrical chamber coupled with a TMP followed by using a mechanical pump which yields a base pressure less than 10^{-7} Torr. The separation between the substrate and the target was about 7 cm. To have uniform film, substrates were kept rotating all through the sputtering process using a stepper motor. Initially, The chamber was evacuated to a high vacuum of 8×10^{-6} Torr using rotary and turbo pumps. The RF power was varied from 50 W to 150 W. To study the effect of the RF power, It varied from 50 to 150 W keeping N_2 concentration constant (2%). On the other hand, to study the effect of the N_2 concentration, the concentration was changed from 1 to 3% at keeping RF power (100W) as a constant. The flow rate of the sputtering gas Ar (99.99% purity) was set to 60 sccm and controlled by a mass flow controller. All samples were deposited under almost the same environment. The deposition rate was maintained constant throughout the sample preparation. Annealing in Ar ambient at 500°C was maintained constant for all the samples after the sputtering to improve the crystalline quality of the samples. The growth condition and post-treatments affect the structural, optical, and morphological properties of grown samples. The base pressure of 8×10^{-6} Torr, deposition time 60 min, RF power 50-150 W, Distance between the substrate holder and target electrode was 7cm and Ar gas flow rate was kept at 60 sccm.

The resulting CdTe layers were studied using a range of relevant techniques for their compositional, morphological, electrical, and optical properties, and hence the optimum growth conditions were established.

4.2.2 Film characterization

Identification of phases and their chemical compositions were investigated using X-ray Diffraction (XRD) by a Stoe XPERT-PRO with Cu K_α radiation excitation wavelength of

1.541 Å. Surfaces Morphology and roughness of samples were observed using Field emission Scanning Electron Microscopy (FESEM), Atomic Force Microscopy (AFM). The FESEM images were taken using the Hitachi S4160, while AFM was carried out using Solver Next, NT-MD.

4.2.3 Computational methodology

Theoretical simulations are accomplished by employing the FP-LAPW approach in the DFT framework as embodied in the WIEN2K package [173, 266, 267]. The values RKmax, Gmax, lmax and K-point were considered as 8, 13, 10,000 respectively. The optical parameters such as the real and imaginary parts of the dielectric function, Eloss, refraction, and extinction indexes, and reflection parameters have been calculated by Kramers–Kroening equations [268, 269] based on the random phase approximation (RPA) [270]. The absorption coefficient, types of transition, optical constant and optical bandgap were determined from these studies for all the series of thin films.

4.3. Results and discussion

4.3.1 Phase Identification and Composition of Layers

4.3.1.1 X-ray Diffraction (XRD)-

X-ray diffraction is widely used as a nondestructive technique for the structural characterization of different materials and identification of material phases, crystallinity, and the size of crystallites within a layer. Figure 4.2 represents the X-ray diffraction (XRD) profile of as-deposited CdTe grown layer at 50, 100, and 150 W RF power and with 1, 2, and 3% nitrogen concentration thin film before and after annealing in the scanning range of 2θ from 20-90^0. The diffraction pattern is dominated by the (111) peak which indicates the preferential growth along a particular crystallographic direction. The broadening of peaks

in XRD indicates the creation of CdTe Nano crystals of small particle size. three peaks at 2θ a 23.48, 38.50, and 46.17 corresponding to (111), (220), and (311) diffraction planes respectively which reveal the character of the polycrystalline cubic structure of CdTe. [271, 272] and one extra peak, which is observed in the XRD spectra, a peak of the CdN_2O_6 (211) plane also appears that confirms the existence of the nitrogen atoms in the CdTe film structure. The result suggests that at 100 W optimized RF power and 2% N_2 concentration to obtain CdTe thin film with moderate crystallinity

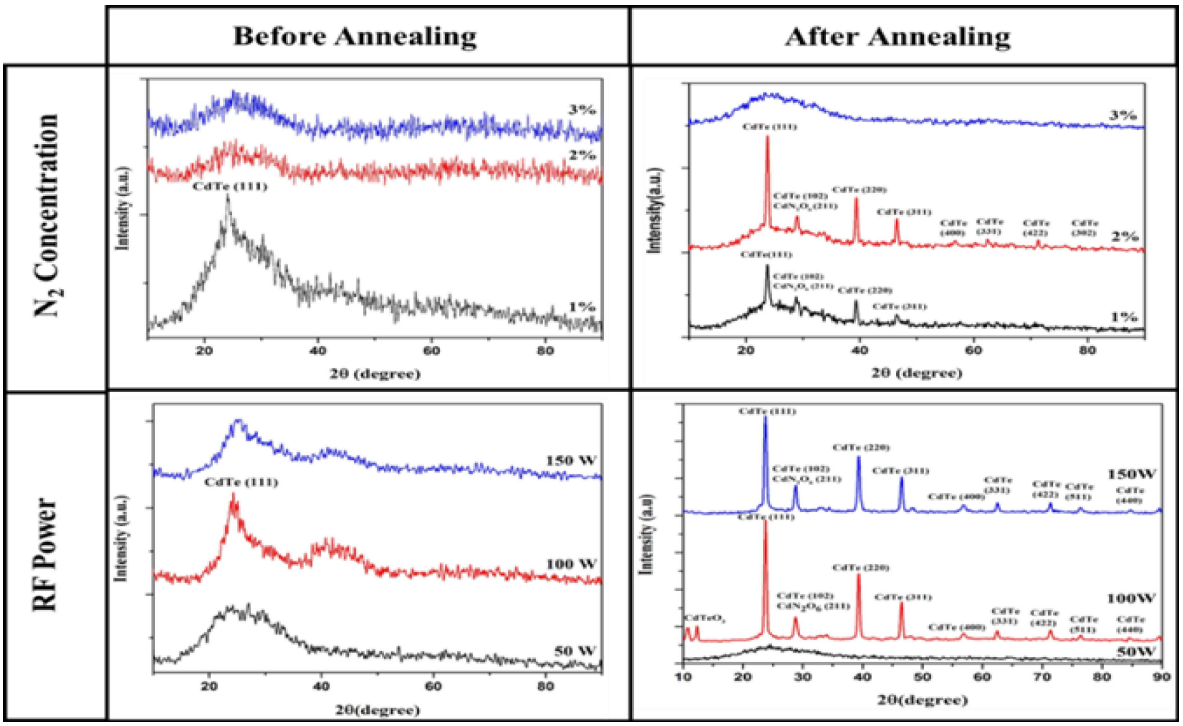

Figure 4.2: XRD spectra of the CdTe films before and after annealing (top shows different N_2 concentrations of 1, 2, and 3% and bottom show different RF powers of 50, 100, and 150 W).

4.3.2 Morphology and Thickness as-deposited annealed thin-films

4.3.2.1 Field emission Scanning Electron Microscopy (FESEM)

It is well known that grain growth and roughness are essential parameters of the absorber layer in thin-film solar cells. To illustrate the Morphology and roughness of the surfaces were observed using field emission Scanning Electron Microscopy (FESEM), Atomic Force Microscopy (AFM). The FESEM images were taken using the same Hitachi S4160 system mentioned above, while AFM measurements were carried out using Solver Next, NT-MD. The surface topography as-deposited and annealed CdTe thin films were taken by atomic force microscopy and the change of surface roughness (average and root-mean-square) with RF power and different N_2 concentration is presented in Figure 4.3 which shows that thickness is the function of RF power. As seen in the figure, grain size and surface roughness increased with increasing the RF power. The grain size increases from 10.4 to 49.8 nm and average roughness increases from 7 to 38.5 nm when RF power increased from 50 to 150W. As indicated by the sputtering theory, the sputtering deposition rate of films is proportional to the sputtering rate of the target and therefore the density of the Ar particle stream. The density of the Ar particle stream increases with an increase in sputtering power. As a result the deposition rate of the target conjointly will increase. Consequently, the growth rate of the film and the thickness of the film will increase with increment in RF power was reported previously by other authors [273,

274].

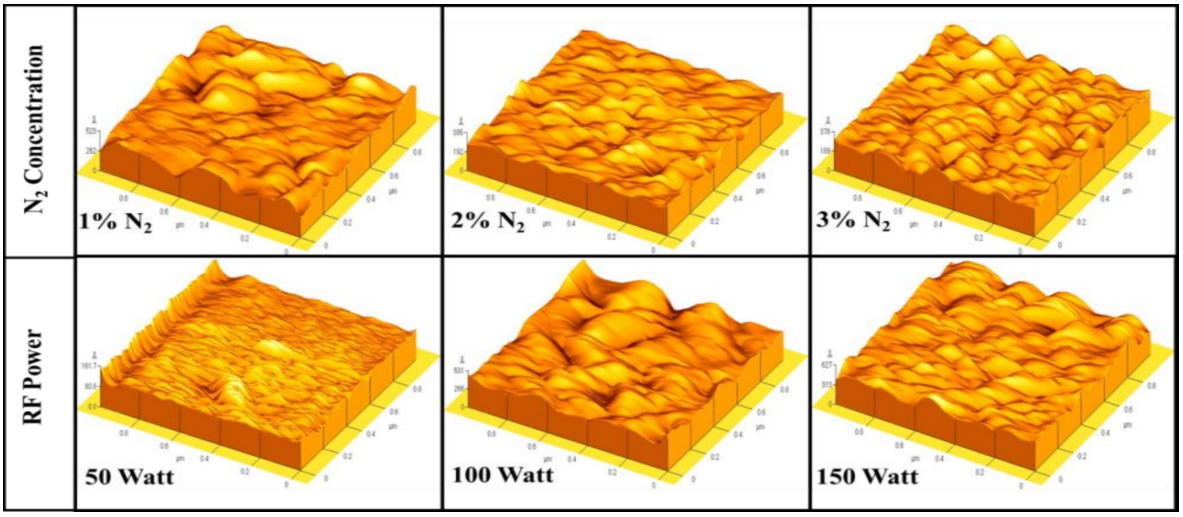

Figure 4.3: AFM images of as-deposited and annealed CdTe thin films (top shows different N_2 concentrations of 1, 2, and 3% and bottom show different RF powers of 50, 100, and 150 W).

Figure 4.4 shows the FESEM images of CdTe thin film, indicating their large area growth reveals the formation crystalline structure. It is observed from the FESEM image that CdTe thin film is homogenous without cracks and covered the substrate surface well. An incremental increase of N_2 concentration leads to the destruction of the surface and the creation of voids and defects in the structure. Moreover, increasing the RF power causes the structure to shift from spherical grains to compress rod structure. CdTe layers deposited by RF power of 100 W with 2% N_2 content in comparison with other deposition conditions show uniformed and denser structure. Hence, these results suggest that 100 W is an optimized RF power of our RF sputtering unit to obtain CdTe thin films with moderate crystallinity and crystallite size.

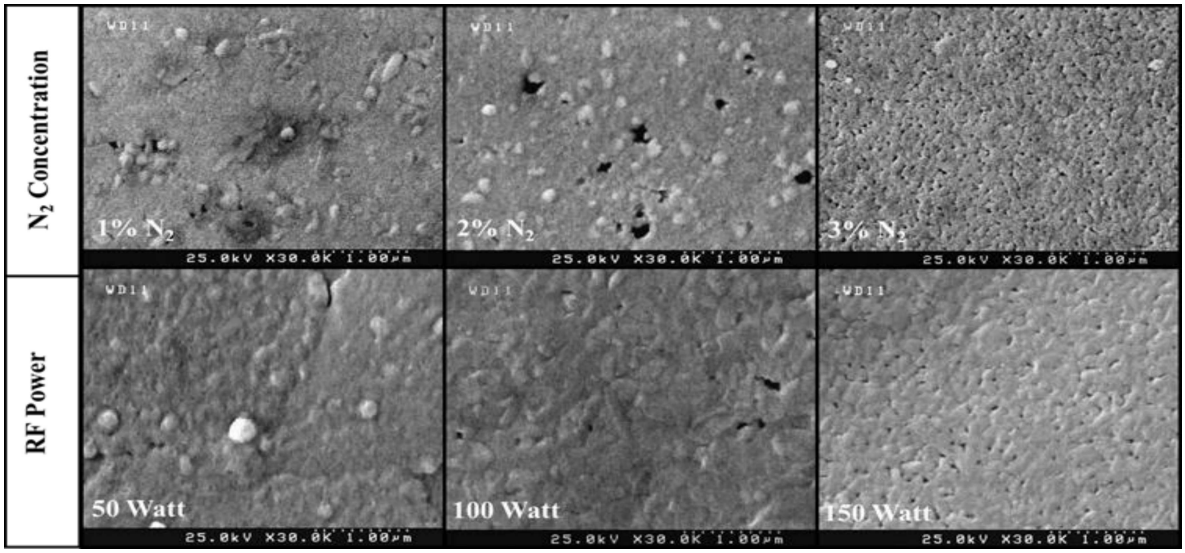

Figure 4.4: FESEM images of CdTe films after annealing (top shows different N_2 concentrations of 1, 2, and 3% and bottom show different RF powers of 50, 100, and 150 W).

4.3.3 UV-Visible spectroscopy analysis

The optical absorption, transmission, and the energy band gap (Eg) of the materials are crucial parameters for the design and development of Photovoltaic devices to achieve improved performance. The reflectance and transmittance spectra of these samples were recorded using by UV-VIS-NIR spectrophotometer (Cary 500 Scan). Once the optical absorption is measured, a Tauc plot can be produced by plotting $(ahv)^2$ versus hv, and then the energy bandgap (the function of hv) can be determined with the help of tauc plot. The bandgap of the CdTe films is calculated from Figure 4.5, which shows the dependence of the absorption coefficient α versus photon energy (hυ) and is given in Table 4.1. Using these data, the absorption coefficient α has been calculated by applying the relation [275]

$$\alpha = \frac{1}{d}\ln\left[\frac{(1-\mathrm{R})^2}{2a} \frac{+[\,(1-R)^4 + 4R^2T^2\,]^{\frac{1}{2}}}{2T}\right]$$

Where d is the thickness of the sample. The absorption coefficient can be written in a general form as a function of incident photon energy hν as [276]

$$\alpha\,(h\upsilon) = \frac{k(h\upsilon - E_g^{opt})^m}{h\upsilon}$$

Where K is the characteristic parameter for the respective transitions [277] hυ is photon energy, E^{opt}_g is the optical energy gap, and m is the number that characterizes the transition process.

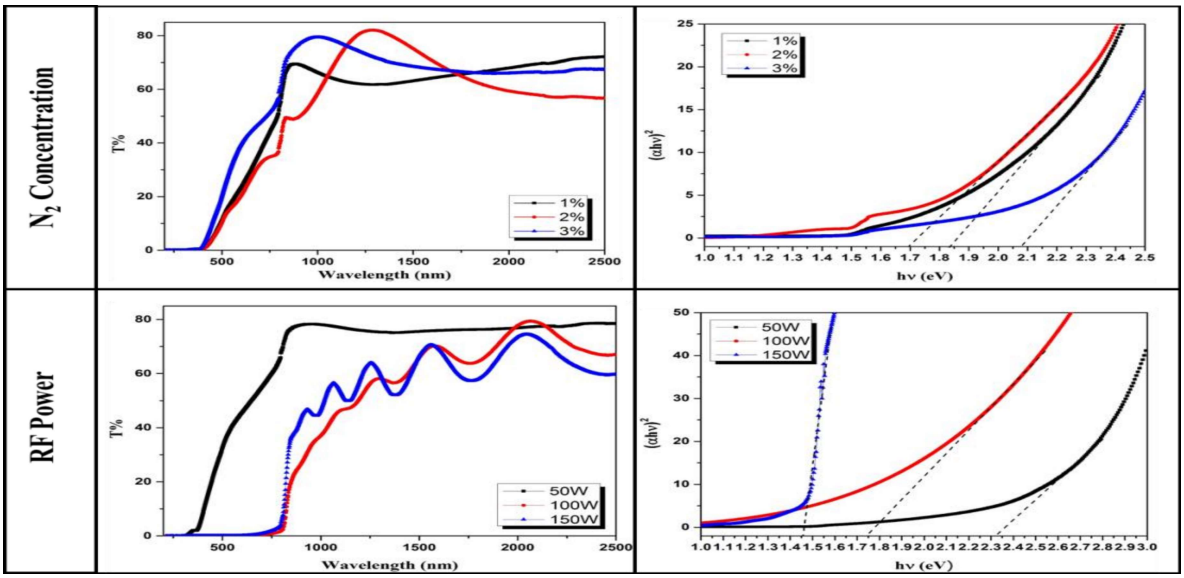

Figure 4.5:a.) UV-Vis optical absorption spectra (left) b.) optical band gap relation plotted between $(ahν)^2$ versus hν (right) for CdTe films after annealing (top shows different N_2 concentrations of 1, 2, and 3% and bottom show different RF powers of 50, 100 and 150 W).

The variation of bandgap as a function of RF power for CdTe thin films deposited using RF sputtering is shown in Figure 4.5. As seen the optical band gap decreases from 2.32 eV to 1.46 eV when the RF power increased from 50 W to 150 W and evaluated bandgap are 1.88ev, 1.69 eV, 2.08ev for the samples at 1% N_2, 2% N_2 and 3% N_2 respectively. These

optical band gap values are in good agreement with the values reported by previous studies. The optical band gap at 100W and 2% N_2 shows an excellent agreement with the reported bulk CdTe band gap value.i.e 1.2-1.7 eV.

Table 4.1: RMS, average roughness, and bandgap values for as-deposited annealed CdTe thin films with different N_2 concentrations of 1, 2, and 3% and RF powers of 50, 100, and 150 W).

After annealing CdTe Films	avg roughness (nm)	RMS roughness (nm)	E_g (eV)
1% N_2	33.4	44.7	1.88
2% N_2	20.0	26.4	1.69
3% N_2	24.6	31.4	2.08
50 W	7.28	10.4	2.32
100 W	38.5	49.1	1.75
150 W	38.5	49.8	1.46

4.3.4 Structural and electronic properties

4.3.4.1 Structural properties

Firstly, the structural properties of CdTe thin films using generalized gradient approximations (GGA) were investigated. The parent $A^{II}B^{VI}$ compounds (CdTe) crystallize in the so-called zinc-blende (ZB) structure which consists of two interpenetrating face-centered cubics (FCC) unit cells. The change unit cell energy versus its cell volume fitted by Brich-Murnaghan equation is depicted in Figure 4.6, which give important information

about the mechanical stability of CdTe compound. It shows a minimum point that is referred to the equilibrium volume and crystal stability in the zince-blende phase. The total energy optimization concerning the lattice parameter, using the Birch-Murnaghan equation via GGA approximation is found to be 6.55A° as shown in Figure 4.6. [278] Then, electronic density of states (DOS) were calculated using using GGA and mBJ approximations which has proven its reliability to successfully simulate the energy gap, thus yielding a better band splitting.

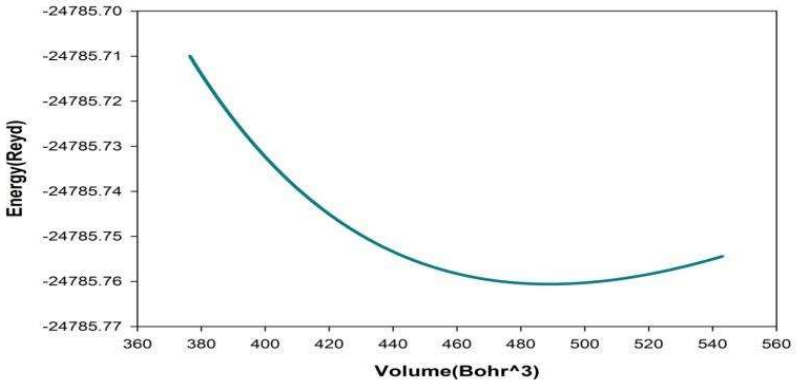

Figure 4.6: The Energy Vs Volume curve of the CdTe using GGA approximation

The calculated total and partial DOS are displayed in Figure 4.7 (a)-(c). In particular, II-VI semiconductor-multilayer structures have recently attracted enormous interest as being suitable for various optoelectronic devices because of direct bandgap covering the whole range of the visible spectrum. From these figures, the sharp states occurring in near the valence band (VB) and conduction band (CB) edges are a consequence of the quantum confinement effect, the valence states are mainly attributed to the p-Te states with a little contribution from the s-Cd states. CdTe is a p-type semiconductor because the Fermi level is

closer to the valence band and states Cd-d and Te-d have no main contribution in the Fermi region.

The DOS of the two mentioned approximations have similar forms, except that in the mBJ approximation, the electronic states have shifted slightly toward higher energies. It is shown that the valance region is divided to two areas with Van-Hov singularity in these edges, relating to the Cd-d and Te-s, p orbitals in the semi-core and -4eV to 0eV regions. The Te-d orbital is the main source for source of the excited electrons to the conduction region.

Table 4.2: The group velocity (V_g (m/s)), the effective electron mass to free electron mass (m^*/m_0) which presented in Fig.8 (b-e) and Energy band gap of CdTe thin film (E_g(eV)).

	V_g (m/s)	m^*/m_0	E_g(eV)
(b) Te-p	5.7139*10^15	-0.0751	
(c) Te-d	-0.3517*10^15	-0.7154	1.57
(d) Cd-s	-0.3158*10^15	-0.6417	
(e) Cd-p	-0.1842*10^15	0.0759	

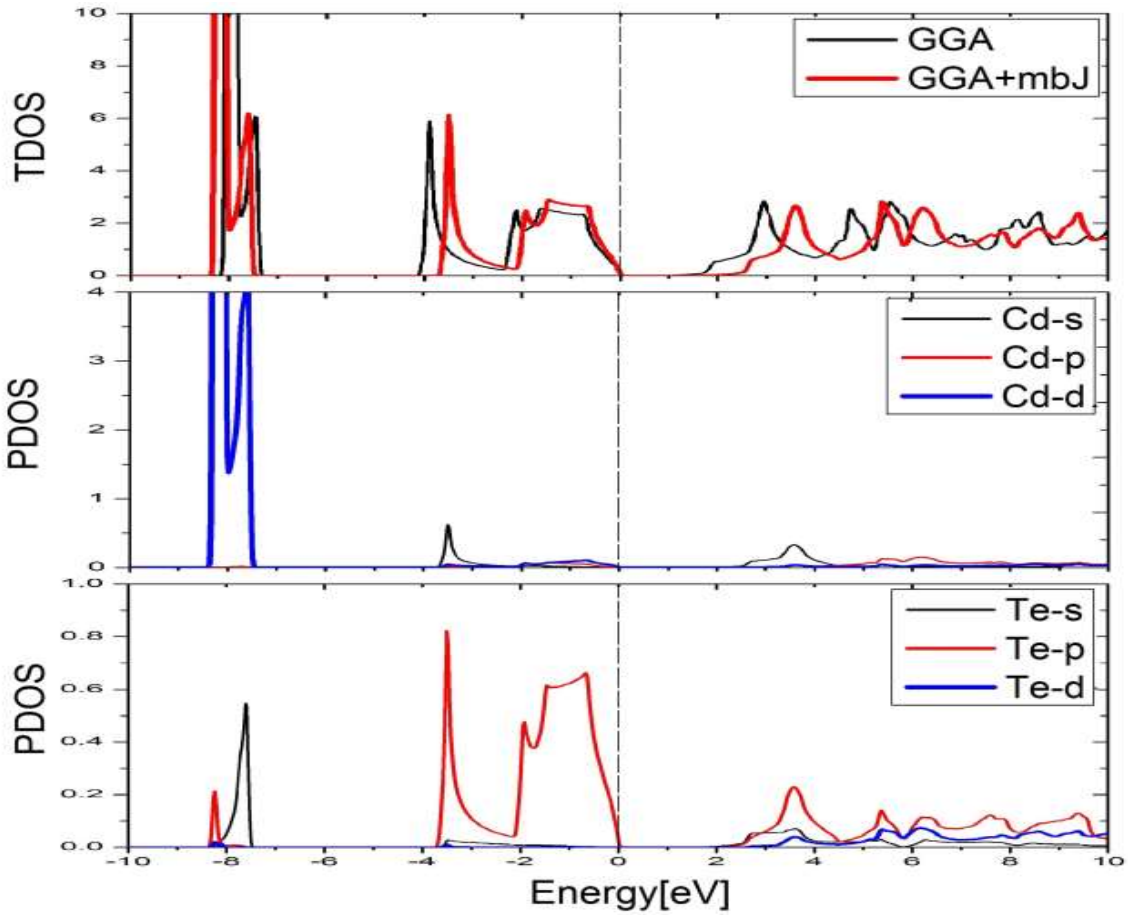

Figure 4.7: (a) The total DOS of CdTe for GGA and MBJ approximations. (b) and (c) represents PDOS of the CdTe orbitals based GGA for Cd and Te respectively.

The calculated band structure of CdTe along the high-symmetry directions of the Brillouin zone (BZ) is shown in Figure 4.8 with a fixed Fermi level, which is in good agreement with previous theoretical work. [279, 280] The Brillouin zone integrations are carried out along Γ, M, K, Γ, A for 3D-CdTe. Each of these bands with their first and second derivatives is plotted in Figure 4.8(b)-4.8(e). Figure 4.8(a) shows that the CdTe has a direct gap in Γ symmetric direction, and at this point, the levels slopes of Fermi level,

especially Te-p in Figure 4.8-b and Cd-s in Figure 4.8-e has a Dirac-like state. As a result, the electron-hole mobility increases strongly so that it can be said that the effective mass in these levels experiences a significant decrease in respect to the electron mass at rest, and similarly, the electron group velocity is large (see Table 4.2). The fundamental band gap investigated via theoretical assumption is 1.57 eV is similar to the experimental value. [281, 282] Therefore, it can be concluded that electron-hole mobility in these levels represents the reaction of this composition against the optical light. Hence, the energy levels of conduction states are dominated by the order of p-orbital energy. It alters the orbital character of the electronic states and, therefore, it affects the optical properties. It is shown that high symmetry and slops around the Γ point, make it as a Γ cones, similar to the graphene structure. So the CdTe has good electron-hole conductivity with high mobility, as we note in the Table 4.2.

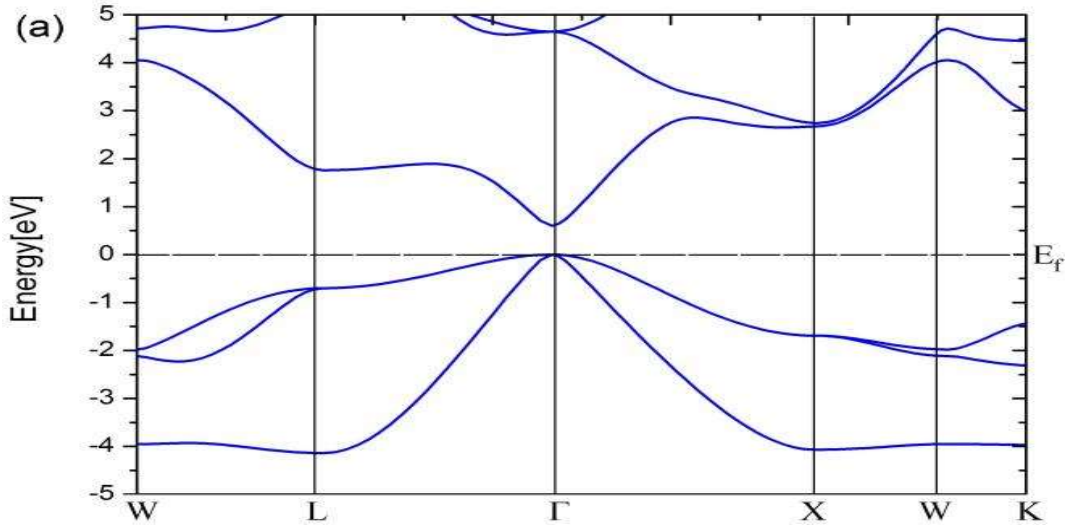

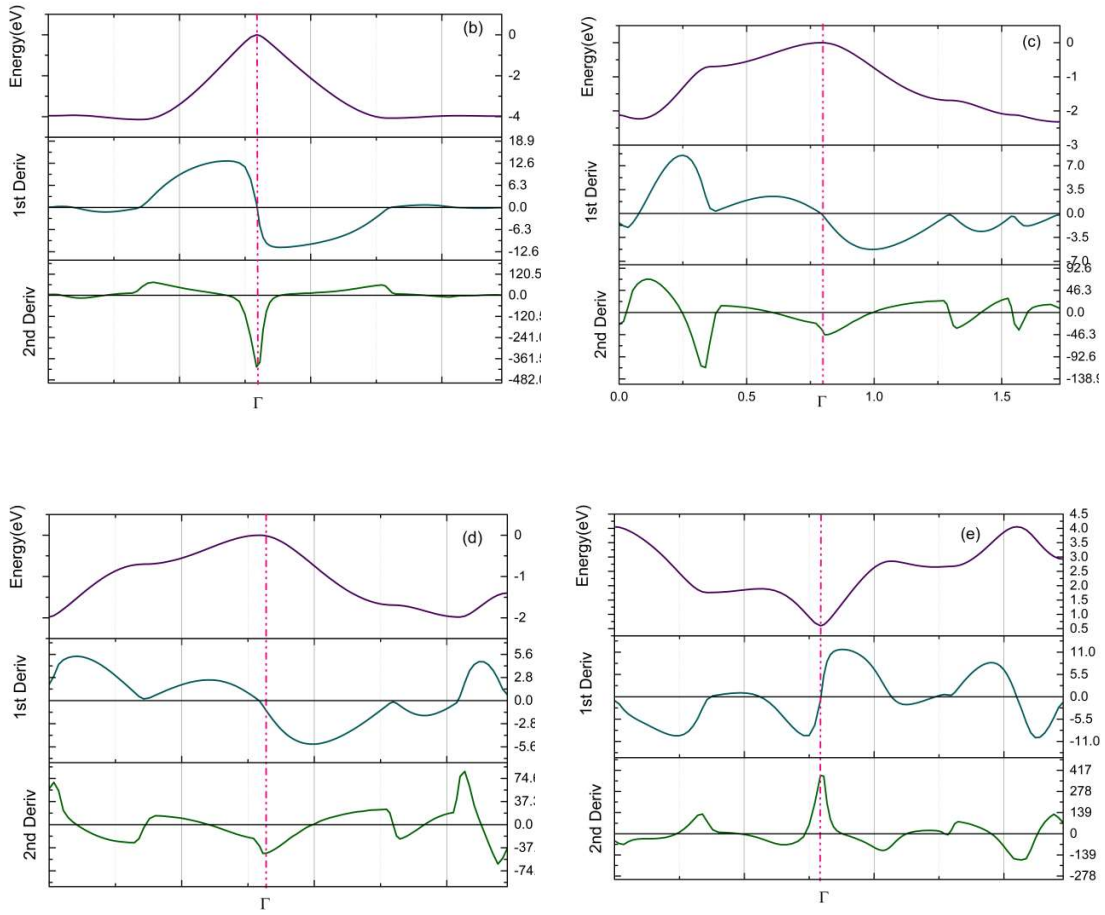

Figure 4.8: (a) The CdTe Band structure for Fermi area levels. (b-e) the level of the (a) part with the 1st and 2nd derivation diagrams.

4.3.4.2 Optical properties

In the process of photovoltaic device development, dielectric function, electron loss function (Eloss), reflectivity and absorption indices, refractive and extinction indices, and optical conductivity of CdTe are crucial parameters to determine and understand using FP-LAPW method [283]within the framework of the random phase approximation (RPA). [270] The RPA provides the frequency-dependent imaginary part of the dielectric tensor is an important factor in the calculation of all-optical parameters. Figure 4.9(a)-4.9(b) shows

the real and imaginary part of a dielectric function using Kramers-kroning relations. [269, 284]

The real and imaginary parts of dielectric function and energy loss function are calculated in figure 4.9 (a), (b) and 4.9(e) respectively. Figure 4.9(a) shows that the real part of the dielectric function becomes zero at the energies of 4.5eV, 6eV, 6.8eV, and 14eV. The negative sign of the real part of the dielectric function means no light passing in that energy area. Figure 4.9(b) shows the imaginary part of the dielectric function $\left(Im - \varepsilon(\omega)\right)$ so that a peak can be seen in the visible region, and two peaks can be observed at energies of 4eV, and 6eV is probably due to the 'parallel band' effect. It signifies that there is a band above E_F that is approximately parallel to another band below CB, the interband transitions from a large number of occupied k states below E_F occur at the same energy, which results in a strong peak.

The energy-loss spectrum in Figure 4.9(e) describes the energy loss of a fast electron traversing the material corresponds to two prominent peaks are observed at 11.8 eV and 14 eV represent the energy of collective excitations of the electronic charge density in the crystal. Figure 4.9(e), especially in 14eV, Plasmon oscillations can be observed. This parameter has not any peak in the infrared and visible area that implying to good optical applications in the lower energies.

The absorption spectra can be described by the process of photon absorption which is due to the excitation of a VB electron to the CB. The computed absorption spectra are depicted in figure 4.9(c) which indicated that the threshold frequency decreases with an increase of layer thickness. The threshold energy in the absorption spectra is shifted to shorter wavelengths (higher energies) when the periodicity order is reduced. An optical absorption

edge exists with a value of 1.57eV which is close to experimental value for conditions of 2% N2 and 100W. Thus, a prominent peak appears only at energies greater than the optical energy gap and the optical absorption could be significant. For determining the electronic characteristics of a variety of material, optical conductivity is believed to be a powerful tool in the range of 0-25 eV.

Optical conductivity is believed to be a powerful probe in determining the electronic characteristics of a variety of materials. In general, if a system is subjected to an external electric field, a redistribution of charges occurs and current is induced. The optical conductivity spectra are generated in the energy range of 0–25 eV. Figure 4.9(d) shows the optical conductivity; the curve represents several peaks due to the bulk Plasmon excitations which are caused by the electronic transitions from the VBs to the CBs. Conductivity increases at once and with a steep slope after this energy, in the visible region, and the UV edge confirming a very good electron-hole mobility capability (As stated in the electronic calculation section). Overall, electronic structure and optical properties suggest the possibility of designing a suitable band structure that offers great potential for application in optical devices like a solar cell.

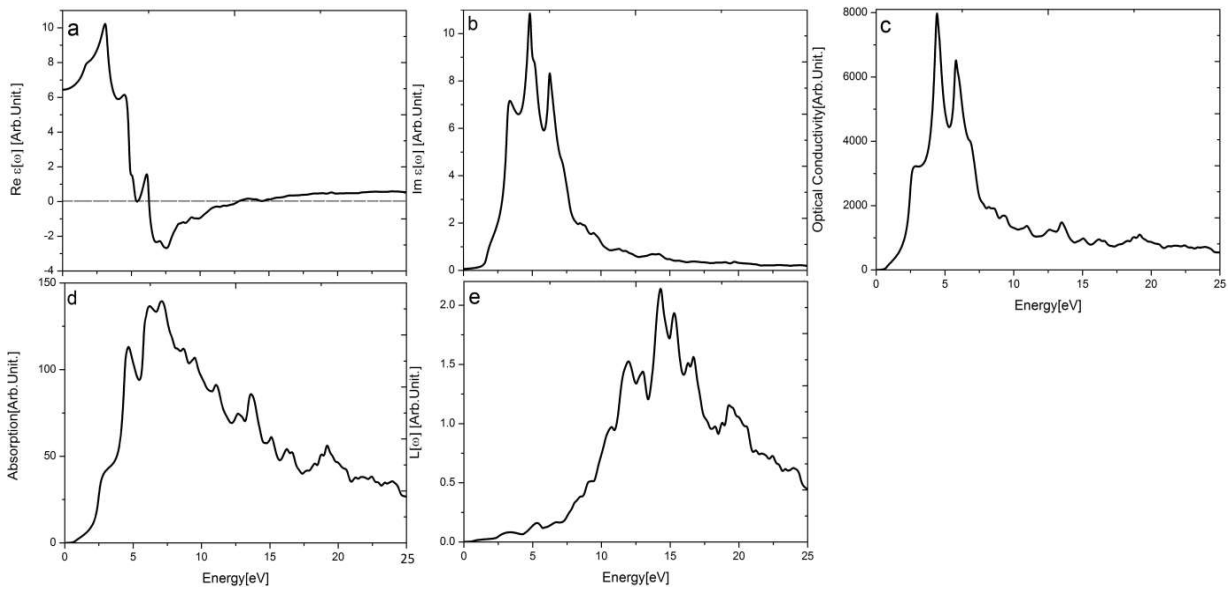

Figure 4.9: (a) , (b) The Real & Imaginary parts of dielectric functions (c) Absorption curve, (d) Optical conductivity and (e) Eloss diagram of CdTe versus photon energy.

4.4. Conclusion

To summarize, we have prepared a series of thin films of CdTe were grown by RF magnetron sputtering at various RF powers and different N_2 concentration and studies the interface through different characterizations. In this chapter, we want to optimize band gap, grain size, and roughness of CdTe so that it can be used as absorber material in photovoltaic applications like a solar cell. Then, the experimental results which will be discussed, in terms of the variation of the semiconductor layer's impact on the bandgap, density of states, and optical characteristics via GGA approximation and MBJ approximation.

Morphological detail and the grain growth were studied from the FESEM and AFM images which show an increase in RF power improves crystallinity in CdTe thin film. The structural analysis revealed that the films were polycrystalline with a predominant zinc-blende structure having higher preferential growth orientation in (111). Moreover, the grain size

increases from 10.4 to 49.8 nm, and average roughness increases from 7 to 38.5 nm when RF power increased from 50 to 150W. A remarkable decrease in the band gap was observed from the UV-visible absorption spectra. The best result shows at 100 W and 2% N_2 which is in excellent agreement with the optimum band gap value. Such optimum band gap CdTe can be used as absorber material in different optoelectronic devices like solar cells.

Additionally, the electronic and optical characteristics are simulated using first-principles calculations. Electron states splitting in the Fermi level is due to Cd-s and Te-p overlapping. The higher electron-hole mobility in the Fermi area belongs to Cd-d and Cd-s orbitals, respectively. The absorption spectra can be described by the process of photon absorption which is due to the excitation of a VB electron to the CB. The dielectric function, electron energy-loss spectrum, absorption coefficient, optical conductivity were also calculated and discussed. Due to the high optical transparency and electrical conductivity along a direction, as well as a variety of novel anisotropic properties, it is a promising material for future applications in display technologies, photovoltaic, and flexible electronics.